Nanoscale

RSC Publishing

COMMUNICATION

View Article Online
View Journal | View Issue

Cite this: *Nanoscale*, 2013, **5**, 10864

Received 28th July 2013
Accepted 2nd September 2013

DOI: 10.1039/c3nr03909a

www.rsc.org/nanoscale

Formation of MS–Ag and MS (M = Pb, Cd, Zn) nanotubes *via* microwave-assisted cation exchange and their enhanced photocatalytic activities†

Yanrong Wang,[a] Wenlong Yang,[a] Lei Zhang,[b] Yong Hu*[a] and Xiong Wen (David) Lou*[b]

A facile microwave-assisted cation-exchange reaction route has been developed to synthesize a series of MS–Ag (M = Pb, Cd, Zn) heterostructure nanotubes (HSNTs) and MS nanotubes. As a demonstration, the as-prepared PbS–Ag HSNTs exhibit significantly enhanced photocatalytic activity for degradation of Congo red and reduction of Cr^{VI}.

Hybrid nanosystems of semiconductors and noble metals have attracted tremendous research attention because of their promising applications in various important fields including photocatalysis, magnetic and electronic storage devices.[1–3] The unique semiconductor–metal interface in this kind of hetero-nanostructure can effectively promote charge carrier transfer and charge separation processes which thereby leads to improved photocatalytic activity.[4,5] Also, the plasmonic metallic components have proved capable of enhancing light absorption of the hybrid system.[6–8] All these effects significantly increase both photocatalytic activity and light-harvesting efficiency of the combined hybrid nanosystems. Motivated by these attractive features, much effort has been devoted to designing and fabricating a wide range of heterostructures with various compositions and structures. As a result, many successful cases of such semiconductor-noble metal nanostructures have been reported with improved photocatalytic activity.[9–12] For example, heterostructures of WO_3 with different metal species have been synthesized and their excellent photocatalytic properties have verified the importance of the metallic components.[13] Among a variety of interesting structures, tubular nanostructures have attracted considerable attention in view of their potential applications in electronics, optoelectronics, catalysis, and controlled release.[14] In particular, heterostructure nanotubes (HSNTs) are recently of particular interest because their multi-functional properties could be further tuned or enhanced by fabricating novel junction modes.[15,16] As an example, we have recently developed a facile one-pot microwave-assisted method to synthesize porous Ag_2S–Ag HSNTs with uniform morphology, good structural stability and high photocatalytic activity.[15] However, there are still some inherent limitations with present synthesis methods, such as structural incompatibility between various materials which usually results in poor stability and uniformity of the synthesized heterostructures.[17,18] Therefore, it is still a great challenge to develop simple and reliable strategies to produce tailored hetero-nanostructured materials.

The cation exchange method, which is a very effective strategy to preserve the starting structures, has been applied to prepare various metal chalcogenide nanostructures.[19] Herein, we report a microwave-assisted cation exchange route for the synthesis of a series of MS–Ag and MS (M = Pb, Cd, Zn) nanotubes. This strategy is facile and rapid, involving only the reaction of Ag_2S–Ag HSNTs or Ag_2S nanotubes with metal cations for 20 min in the presence of tributylphosphine (TBP), and the detailed experimental procedure is provided in the ESI†. The schematic illustration of this method for the synthesis of MS–Ag HSNTs or MS nanotubes is shown in Fig. 1. In the reaction, TBP binds to Ag^+ from the precursor lattice to form intermediate complexes, which facilitate the cation exchange reaction under microwave irradiation. Unlike Ag^+, metallic Ag^0 does not react with TBP, and can therefore be preserved in the resulting structures. The involved reactions with microwave irradiation might be described as follows.[20]

$$Ag_2S\text{–}Ag\ (s) + M^{2+} + 4TBP \rightarrow 2[Ag(TBP)_2]^+ + MS\text{–}Ag\ (s)\ (M = Pb, Cd, Zn)$$

The crystallographic structure and phase purity of the as-prepared porous MS–Ag HSNTs and MS nanotubes are

[a]*Key Laboratory of the Ministry of Education for Advanced Catalysis Materials, Institute of Physical Chemistry, Zhejiang Normal University, Jinhua, 321004, P. R. China. E-mail: yonghu@zjnu.edu.cn*

[b]*School of Chemical and Biomedical Engineering, Nanyang Technological University, 62 Nanyang Drive, Singapore 637459, Singapore. E-mail: xwlou@ntu.edu.sg; davidlou88@gmail.com; Web: http://www.ntu.edu.sg/home/xwlou*

† Electronic supplementary information (ESI) available: Detailed experimental procedures, additional SEM/TEM images, XRD patterns, EDS elemental mapping, and fluorescence spectra. See DOI: 10.1039/c3nr03909a

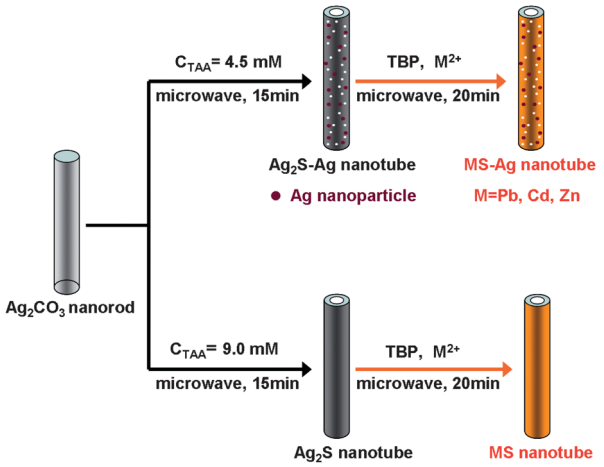

Fig. 1 Schematic illustration of the fabrication process of porous MS–Ag (M = Pb, Cd, Zn) HSNTs and MS nanotubes *via* a facile microwave-assisted cation-exchange route.

examined by X-ray powder diffraction (XRD). As shown in Fig. 2, for all MS–Ag HSNTs, the diffraction peaks in the XRD patterns marked with squares can be assigned to the face-centered cubic Ag (JCPDS card no. 87-0720; space group: *Fmm*, $a = b = c =$ 4.077 Å). The other diffraction peaks can be well indexed to cubic PbS (JCPDS card no. 05-0592; space group: *Fmm*, $a = b = c = 5.936$ Å), hexagonal CdS (JCPDS card no. 41-1049; space group: $P6_3mc$, $a = b = 4.141$ Å, and $c = 6.720$ Å), and wurtzite ZnS (JCPDS card no. 36-1450; space group: $P6_3mc$, $a = b =$ 3.821 Å, and $c = 6.257$ Å). No additional peaks are detected in all the XRD patterns, indicating the high purity of the products. Also the Ag_2S peaks are no longer observed, which indicates complete cation exchange between Ag^+ in Ag_2S–Ag HSNTs and M^{2+} (M = Pb, Cd, Zn) in solution under microwave irradiation for 20 min. The XRD results of the precursor Ag_2S–Ag HSNTs and Ag_2S nanotubes, and MS nanotubes obtained from Ag_2S nanotubes are provided in Fig. S1 (see ESI†).

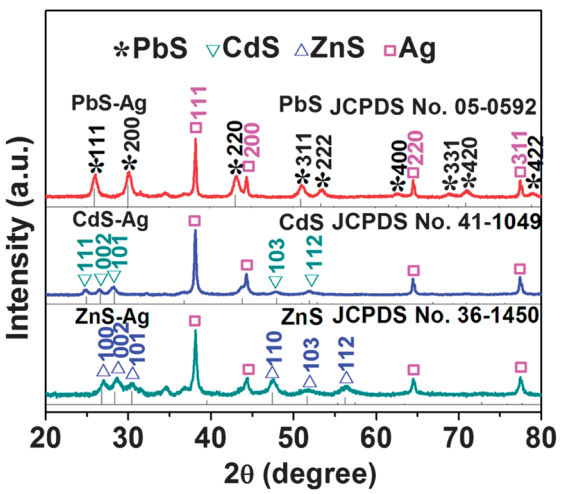

Fig. 2 XRD patterns of the as-prepared porous MS–Ag HSNTs (M = Pb, Cd, Zn).

A scanning electron microscope (SEM) and a transmission electron microscope (TEM) are employed to characterize the morphology and structural details of the as-prepared porous MS–Ag HSNTs and MS nanotubes. Fig. 3 displays the SEM images of the porous MS–Ag HSNTs obtained from the microwave-assisted cation exchange. These images depict porous nanotubes of uniform size, about 100–150 nm in diameter and 1–2 μm in length, which is the same as the size of the Ag_2S–Ag precursor (Fig. S2, ESI†). One can see that the preserved structures are quite pure, without any impurity particles or aggregates. Similar features are also observed in the MS nanotubes (Fig.S3, ESI†). The geometrical structures of the porous MS–Ag HSNTs are further elucidated by TEM observation. As can be seen in Fig. 4a, c and e, the MS–Ag HSNTs well duplicate the size and shape of the Ag_2S–Ag nanotubes. Fig. 4b, d and f show the corresponding high-resolution (HR) TEM images of these MS–Ag HSNTs, which clearly reveal the heterojunction region between the MS semiconductor and Ag metal. This result further confirms that the cation exchange reaction between M^{2+} and Ag^+ in Ag_2S–Ag is completely realized *via* this facile and rapid microwave-assisted method. Additionally, the SEM images of the MS nanotubes are shown in Fig. S3 (see ESI†), which also illustrates the intact nanotube structures. Spatial distribution of the compositions in MS–Ag HSNTs is further studied by elemental mapping. The mapping results reveal uniform distribution of Ag and M (M = Pb, Cd, Zn) throughout the HSNTs (Fig. S4–6, ESI†). It can be seen that the size of the primary MS and Ag nanocrystals in the HSNTs is relatively large. As a result, the Brunauer–Emmett–Teller (BET) specific surface area of the as-obtained PbS–Ag HSNTs is only about 16.7 $m^2\ g^{-1}$.

Recent studies have suggested that semiconductor-Ag heterostructures might possess advantages such as favorable charge separation and a wide absorbance range of light.[21,22] In the present work, we characterize the photocatalytic properties of these new types of porous HSNTs as promising photocatalysts. Using PbS–Ag HSNTs as an example, we carry out the photocatalytic degradation experiments of organic dye Congo red (CR) and the reduction tests of Cr^{VI} species in an aqueous solution under visible-light irradiation. Fig. 5 shows the photocatalytic activity results of the PbS–Ag HSNTs and PbS nanotubes. Fig. 5a displays the photocatalytic degradation of CR by blank, P25, as-prepared PbS–Ag HSNTs and PbS nanotubes, where C is the concentration of CR after different light irradiation times and C_0 is the concentration of CR after reaching adsorption/desorption equilibrium in the dark. After visible-light irradiation for 60 min, nearly 75.2% of CR is

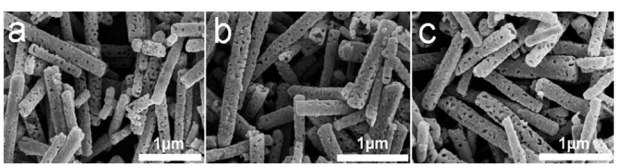

Fig. 3 SEM images of (a) PbS–Ag, (b) CdS–Ag, and (c) ZnS–Ag HSNTs.

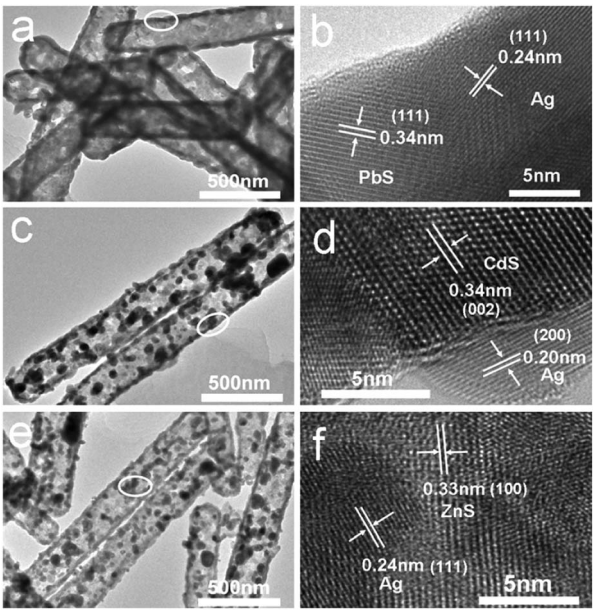

Fig. 4 TEM and HRTEM images of the as-obtained MS–Ag HSNTs: (a and b) PbS–Ag, (c and d) CdS–Ag, and (e and f) ZnS–Ag.

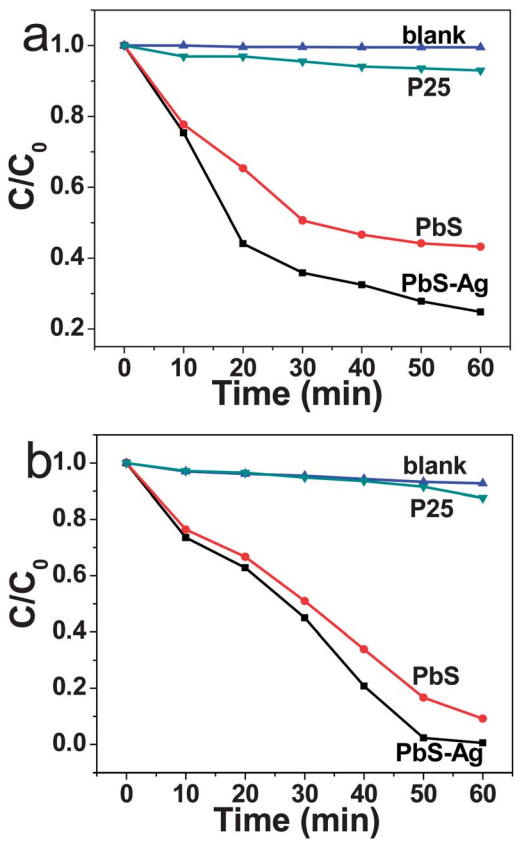

Fig. 5 (a) Photocatalytic degradation of CR and (b) reduction of Cr^{VI} using the as-obtained PbS–Ag HSNTs, PbS nanotubes and P25 as photocatalysts.

degraded by the PbS–Ag HSNT sample, whereas other samples exhibit relative lower activities, namely 7.3% for P25 and 56.7% for PbS nanotubes. Fig. 5b shows the photocatalytic reduction of Cr^{VI} under visible-light irradiation. Again the PbS–Ag sample exhibits the highest photocatalytic activity. The superior photocatalytic performance of porous PbS–Ag HSNTs may be ascribed to the enhanced charge-transfer process in the hybrid nanostructures. The work function of Ag and the bottom of the conduction band of PbS are 4.26 and 4.5 eV, respectively, relative to the vacuum energy level.[23,24] Benefitting from the closely located energy levels, photoexcited electrons in the conduction band of PbS can transfer to Ag in the hybrid nanostucture easily, leading to high-efficiency charge separation. The effective charge separation therefore increases the photocatalytic activity of the PbS semiconductor by suppressing the recombination process of the photoexcited electrons and holes.[25] This accounts for the observed superior activity of PbS–Ag HSNTs over other photocatalysts. The photocatalytic reduction of Cr^{VI} using the as-obtained CdS–Ag and ZnS–Ag HSNTs as photocatalysts is also shown in Fig. S7 (see ESI†). After visible-light irradiation for 60 min, about 56% and 15% of Cr^{VI} can be degraded by the as-prepared CdS–Ag and ZnS–Ag HSNTs, respectively. Furthermore, the ·OH radicals formed in the photocatalytic process can be probed using a method described previously.[26] It is well known that ·OH reacts with terephthalic acid (TA) in a basic solution to generate 2-hydroxy-terephthalic acid (TAOH) which emits characteristic fluorescence centered at 426 nm.[27] As shown in Fig. S8 (see ESI†), significant fluorescent signals associated with TAOH are observed from different photocatalysts suspended in a TA solution upon visible-light irradiation for 10 min. The result clearly demonstrates that the photoexcited holes are powerful enough to oxidize surface adsorbed hydroxy groups and water molecules to generate ·OH radicals. Additionally, a maximum number of ·OH radicals are formed by using the PbS–Ag HSNT photocatalyst in the photoreaction process; which is in good agreement with the above results of CR photodegradation and Cr^{VI} photoreduction. Further, the UV-vis diffuse reflectance spectra of the as-prepared PbS–Ag HSNTs and PbS nanotubes are shown in Fig. S9 (see ESI†). It can be clearly seen that PbS–Ag HSNTs absorb much more visible light than PbS nanotubes, which might be attributed to the surface plasmon resonance effect of Ag.

In summary, we have developed a rapid microwave-assisted cation-exchange method to synthesize a series of porous MS–Ag HSNTs and MS nanotubes. As an example, the as-prepared PbS–Ag HSNTs exhibit excellent photocatalytic activity for both photodegradation of Congo red and the photoreduction of aqueous Cr^{VI}. The synergistic effect between semiconductor PbS and Ag has also been investigated through the generation of ·OH radicals in PbS–Ag HSNTs. This work provides an excellent example of fabricating functional semiconductor–metal heterostructures with a variety of compositions and uniform morphology for different applications.

Acknowledgements

Financial support from the Natural Science Foundation of China (21171146) is gratefully acknowledged by Y. Hu.

Notes and references

1 X. H. Li, J. Lian, M. Lin and Y. T. Chan, *J. Am. Chem. Soc.*, 2011, **133**, 672–675.
2 G. Oldfield, T. Ung and P. Mulvaney, *Adv. Mater.*, 2000, **12**, 1519–1522.
3 N. L. Kovtyukhova and T. E. Mallouk, *Adv. Mater.*, 2005, **17**, 187.
4 V. Subramanian, E. E. Wolf and P. V. Kamat, *J. Am. Chem. Soc.*, 2004, **126**, 4943–4950.
5 M. Jakob, H. Levanon and P. V. Kamat, *Nano Lett.*, 2003, **3**, 353–358.
6 R. Costi, A. E. Saunders, E. Elmalem, A. Salant and U. Banin, *Nano Lett.*, 2008, **8**, 637–641.
7 E. Formo, E. Lee, D. Campbell and Y. N. Xia, *Nano Lett.*, 2008, **8**, 668–672.
8 K. Awazu, M. Fujimaki, C. Rockstuhl, J. Tominaga, H. Murakami, Y. Ohki, N. Yoshida and T. Watanabe, *J. Am. Chem. Soc.*, 2008, **130**, 1676–1680.
9 T. Mokari, E. Rothenberg, I. Popov, R. Costi and U. Banin, *Science*, 2004, **304**, 1787–1790.
10 S. Chakrabortty, J. A. Yang, Y. M. Tan, N. Mishra and Y. T. Chan, *Angew. Chem., Int. Ed.*, 2010, **49**, 2888–2892.
11 S. E. Habas, P. D. Yang and T. Mokari, *J. Am. Chem. Soc.*, 2008, **130**, 3294.
12 E. Elmalem, A. E. Saunders, R. Costi, A. Salant and U. Banin, *Adv. Mater.*, 2008, **20**, 4312–4317.
13 G. C. Xi, J. H. Ye, Q. Ma, N. Su, H. Bai and C. Wang, *J. Am. Chem. Soc.*, 2012, **134**, 6508–6511.
14 Y. Yang, D. S. Kim, M. Knez, R. Scholz, A. Berger, E. Pippel, D. Hesse, U. Gosele and M. Zacharias, *J. Phys. Chem. C*, 2008, **112**, 4068–4074.
15 W. L. Yang, L. Zhang, Y. Hu, Y. J. Zhong, H. B. Wu and X. W. Lou, *Angew. Chem., Int. Ed.*, 2012, **51**, 11501–11504.
16 Y. P. Bi and J. H. Ye, *Chem. Commun.*, 2010, **46**, 1532–1534.
17 Y. J. Hwang, A. Boukai and P. D. Yang, *Nano Lett.*, 2009, **9**, 410–415.
18 T. Ghoshal, S. Biswas and S. Kar, *J. Phys. Chem. C*, 2008, **112**, 20138–20142.
19 D. H. Son, S. M. Hughes, Y. D. Yin and A. P. Alivisatos, *Science*, 2004, **306**, 1009–1012.
20 J. T. Zhang, Y. Tang, K. Lee and M. Ouyang, *Science*, 2010, **327**, 1634–1638.
21 F. R. Jiang, Q. W. Tian, M. H. Tang, Z. G. Chen, J. M. Yang and J. Q. Hu, *CrystEngComm*, 2011, **13**, 7189–7193.
22 S. L. Wang, H. H. Qian, Y. Hu, W. Dai, Y. J. Zhong, J. F. Chen and X. Hu, *Dalton Trans.*, 2013, **42**, 1122–1128.
23 J. S. Lee, E. V. Shevchenko and D. V. Talapin, *J. Am. Chem. Soc.*, 2008, **130**, 9673.
24 B. Levy, in *Photochemical Conversion and Storage of Solar Energy*, Springer, New York, 1990.
25 M. L. Pang, J. Y. Hu and H. C. Zeng, *J. Am. Chem. Soc.*, 2010, **132**, 10771–10785.
26 Y. Liu, Y. Hu, M. J. Zhou, H. S. Qian and X. Hu, *Appl. Catal., B*, 2012, **125**, 425–431.
27 G. Liu, P. Niu, L. C. Yin and H. M. Cheng, *J. Am. Chem. Soc.*, 2012, **134**, 9070–9073.